

Dynamic continuous recrystallization characteristics in two stage deformation of Mg–3Al–1Zn alloy sheet

J.C. Tan, M.J. Tan*

School of Mechanical and Production Engineering, Nanyang Technological University, Nanyang Avenue, Singapore 639798, Singapore

Received 31 August 2001; received in revised form 31 January 2002; accepted 7 February 2002

Abstract

Dynamic recrystallization (DRX) characteristics of a Mg–3Al–1Zn (AZ31) alloy sheet were investigated at temperatures ranging from 200 ~ 450 °C and constant strain rates of $1 \times 10^{-4} \sim 2 \times 10^{-4} \text{ s}^{-1}$. The average grain size of the as-received alloy was 12 μm and can be refined to 6 μm via deformation at 250 °C, $1 \times 10^{-4} \text{ s}^{-1}$ to a strain level of 60%. Grain refinement was less effective at higher temperatures due to rapid grain growth. The grain refinement was attributed to dynamic continuous recrystallization which involves progressive increase in grain boundary misorientation and conversion of low angle boundaries into high angle boundaries. During DRX, subgrains were developed through the conversion of dislocation cell walls into subgrain boundaries. The presence of precipitates was not essential for dynamic recrystallization in the magnesium alloy being investigated because of its limited slip systems, low stacking fault energy and high grain boundary diffusion rate.

© 2003 Elsevier Science B.V. All rights reserved.

Keywords: Magnesium alloy; Dynamic recrystallization; Grain refinement; Subgrains; Superplasticity

1. Introduction

The greatest advantage of choosing magnesium alloys for engineering designs lies in its low density, which translates into higher specific mechanical properties. These favorable properties can contribute significantly to the aspect of weight savings in the design and construction of automotive and aerospace components, materials handling equipments, portable tools and even sporting goods [1,2]. However, magnesium alloys have poor formability and limited ductility at room temperature ascribed to their hexagonal close-packed (HCP) crystal structure. As a result, to date, the majority of the structural magnesium products is fabricated by die-casting process [3] instead of employing plastic forming techniques such as rolling, forging and extrusion [4]. Consequently, it is imperative to improve the poor workability of wrought magnesium alloys via superplastic deformation in order to facilitate wider structural applications.

Takuda and his coworkers [5] reported that the superplasticity of a Mg–1.86Al–0.79Zn (in wt.%) alloy sheet was substantially improved by first refining the grains of the rolled alloy through predeformation process. A maximum elongation-to-failure, ϵ_f , of 345% was reported. However, their paper did not elucidate the essential deformation mechanisms underlying the tensile elongation improvement. Very recently, Mohri et al. [6] have demonstrated that a rolled Mg–9Al–1Zn (in wt.%) alloy could be made to deform superplastically after going through dynamic recrystallization (DRX) which resulted in a fine grain structure. A maximum elongation of 604% was attained after grain refinement. DRX of other superplastic materials such as Co₃Ti [7] and Duralumin (D-19) [8] was also reported and was revealed to be effective in improving the elongation-to-failure. However, the literature and data available on DRX of superplastic magnesium alloy sheets are extremely limited; hence their microstructural evolutions as well as the governing deformation mechanisms are not well understood.

Earlier work by the present authors [9] found that the optimum superplastic deformation conditions for a rolled Mg–3Al–1Zn sheet were at 450 °C and $2 \times$

* Corresponding author. Tel: +65-790-5582; fax: +65-791-1859
E-mail address: mmjtan@ntu.edu.sg (M.J. Tan).

10^{-4} s^{-1} , which attained a maximum elongation-to-failure of 265% and strain rate sensitivity (m) of 0.3, signifying Class-I solid solution alloy. Even though the specimen initially possessed a relatively fine microstructure, it eventually coarsened due to rapid grain growth at elevated temperature. The resultant coarse-grained structure was shown to deform by viscous glide mechanism accommodated by lattice diffusion. In the present paper, DRX phenomenon in a rolled Mg–3Al–1Zn alloy is investigated and subsequently in the companion paper [10], it is demonstrated how DRX can be exploited to enhance superplasticity by employing a two stage deformation method.

2. Experimental procedures

The magnesium alloy used in this study was a commercial Mg–3Al–1Zn (AZ31B-O) cross-rolled sheet, whose chemical composition is listed in Table 1. The as-received material had an average grain size of 12 μm determined by the linear intercept method [11] using an image analyzer software. Tensile specimens with a gauge of 15 mm length, 4 mm width and 2 mm thickness were electro-discharged machined with the tensile axis parallel to the final rolling direction. Prior to testing, all specimens were polished using diamond paste to 6 μm surface finish to remove major scratches.

The elevated temperature tensile tests were performed in an Instron-4206 universal testing machine equipped with electrical resistance furnace which can maintain a temperature variation of $\pm 2\text{K}$. The tests were performed in air at atmospheric pressure and employing constant strain rates. The time required to raise the temperature to the desired value greatly depended on the test temperature, which could range from 20 to 60 min. All tests were conducted by first heating up each specimen to the desired temperature, followed by a 20-min holding time to ensure thermal equilibrium. Prior to straining, the temperature of the specimen was further verified using a thermocouple put in contact with the gauge of the specimen. The variation of stress and strain was monitored continuously by a personal computer equipped with an automatic data acquisition system. All tests were repeated three times and the average values were calculated. The elongation-to-failure, ε_f , was obtained from the gauge length of the fractured specimen.

In order to preserve the microstructures, at the specified strain or at fracture, samples were immediately unloaded and quenched in water. Specimens for optical microscopy were sectioned, cold mounted, polished and then etched in acetic picral [5 ml acetic acid + 6g picric acid + 10 ml H_2O + 100 ml ethanol (95%)]. The grain size measurement was done using the optical microscope and image analyzer software. The ‘Heyn’ lineal intercept procedure [11] which can be used for counting equiaxial grains as well as distinctly non-equiaxed microstructures was employed.

A scanning electron microscope (SEM) was utilized to investigate the surface morphology of specimens while the interior microstructure of grains was examined under a transmission electron microscope (TEM). Specimens for TEM were prepared by first ground-polishing the sample to about 100 μm thickness foil followed by punching of 3 mm diameter disks. A Gatan dimple grinder was then used to mechanically thin the disks to a minimum thickness of 15 ~ 20 μm , followed by perforation using Gatan’s Precision Ion Polishing System.

3. Results and discussion

3.1. Effects of temperature and strain rate on dynamic recrystallization (DRX)

The temperature range of 200 ~ 400 $^{\circ}\text{C}$ and constant strain rates ranging from low to high, i.e. $1 \times 10^{-4} \sim 1 \times 10^{-2} \text{ s}^{-1}$ were chosen for DRX studies. ‘Fine’ grains are defined as grains having an average diameter of $\leq 10 \mu\text{m}$ and the volume fraction of fine grains V_f is defined as follows:

$$V_f = \frac{\text{Total area of individual fine grains, } \sum A_f}{\text{Total sampling area, } \sum A_i} \quad (1)$$

It is essential to quantify the grain size based on either the area of individual fine grain, A_f or the average grain diameter, \bar{d} because of the non-homogenous nature of grain distribution resulted from incomplete DRX. Average grain measurement was carried out on at least 5000 grains for improved reliability. The large grain size is not suitable for grain boundary sliding (GBS) in view of the fact that in general only grains with an average size of less than 10 μm and possess high misorientation angles can deform by GBS [12,13]. All the fine grains observed at fracture within the gauge region can be

Table 1
Chemical composition (wt.%) of Mg–3Al–1Zn alloy

Mg	Al	Zn	Mn	Fe	Ni	Cu	Si	Pb	Sn	Ca
Bal.	2.5–3.5	0.7–1.3	0.2 min.	0.002 max.	0.001 max.	0.002 max.	0.02 max.	0.01 max.	0.01 max.	0.002 max.

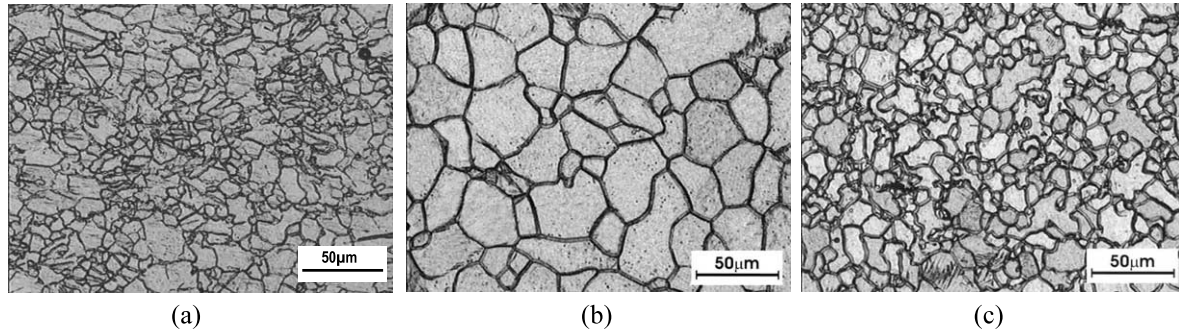


Fig. 1. (a) Microstructure of as-received alloy. Isochronous microstructures at the (b) grip and (c) gauge regions obtained from the same fractured specimen tested at 250 °C and $1 \times 10^{-4} \text{ s}^{-1}$. The tensile axis was horizontal.

presumed as new grains that have been dynamically recrystallized under the influence of stress and elevated temperature. This assumption is valid since the isochronous grains at the grip of the specimen that were not under the influence of stress coarsened, as shown in Fig. 1, in contrast to the fine grains found along the gauge.

The effects of employing different combinations of temperature and strain rate on the percentage of fine grains attainable at fracture are clearly depicted in Fig. 2. The highest volume fraction of fine grains attainable was 92%, when deformation was performed at 250 °C and $1 \times 10^{-4} \text{ s}^{-1}$. When the test temperature was increased to 300 and 350 °C, specimens had to be deformed at higher strain rates, in the order of $\times 10^{-3}$ and $\times 10^{-2}$ to attain high percentage (i.e. >50%) of fine grains. It can be observed that 70% and 60% of dynamically recrystallized grains could be obtained at 300 °C, $1 \times 10^{-3} \text{ s}^{-1}$ and 350 °C, $1 \times 10^{-2} \text{ s}^{-1}$, respectively.

As anticipated, grain refinement by dynamic recrystallization becomes less effective at higher temperatures, i.e. 400 °C (and above) for the chosen strain rate range due to rapid grain growth which offsets the positive effects of DRX. Consequently, the percentage of fine grains attainable never exceeded 15% for all the chosen strain rates. Conversely, it was also difficult to achieve high volume fraction of fine grains at 200 °C and higher

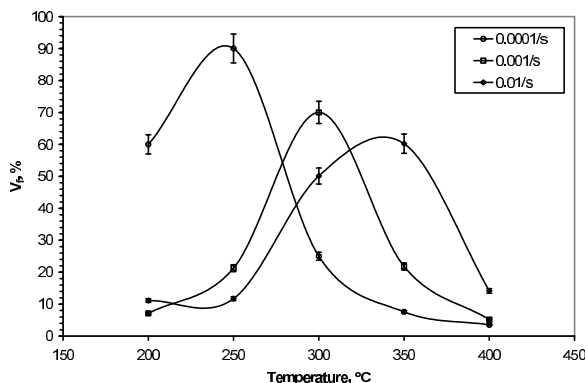


Fig. 2. Volume fraction of fine grains attainable at fracture plotted against temperature, for the three strain rates.

strain rates since dynamic recrystallization rate was greatly reduced by the relatively low temperature. Moreover, due to the fact that specimen which deformed at higher strain rates failed at lower elongation-to-failure; hence DRX process was interrupted before its completion.

The above result is summarized in Table 2, presenting the three feasible routes for grain refinement of a rolled Mg–3Al–1Zn alloy via DRX. Apparently, Route I is the most favorable course for achieving grain refinement, which yielded the highest percentage of homogeneous fine grains ($\approx 92\%$) and the smallest average grain size ($\approx 6.5 \mu\text{m}$) together with a relatively high elongation-to-failure. The microstructural evolution during deformation at 250 °C and constant strain rate of $1 \times 10^{-4} \text{ s}^{-1}$ was further investigated with the aim at determining the optimum strain for attaining optimum percentage of fine grains. Specimens were deformed to strains, ϵ , of 5, 20, 40, 60 and 100%, and the resulting microstructures as well as grain size distributions were recorded.

Fig. 3 presents a typical true stress versus tensile strain curve of a specimen deformed at 250 °C and constant strain rate of $1 \times 10^{-4} \text{ s}^{-1}$. The flow stress increased rapidly upon loading and reached a maximum value of $\approx 48\text{MPa}$ at 20% strain. It was reported [14,15] that superplastic materials with fine-grained microstructure prior to tensile tests exhibit apparent strain hardening and no apparent strain softening behavior during the initial stage of test. This apparent strain hardening behavior is claimed to be attributed to grain growth. For the current alloy, substantial grain growth (see Fig. 4(a)) at the initial stage of deformation explains the strain hardening phenomenon. Subsequently, a gradual decrease in flow stress could be observed when deformation proceeded from 20 to 40%. The strain softening behavior was attributed to the initiation of dynamic recrystallization, as revealed by Fig. 4(c). Furthermore, a steady state flow was attained after about 50% strain and had a magnitude of approximately 45 MPa. The alloy exhibited a steady state flow behavior which normally can only be attained at temperatures greater

Table 2

Feasible dynamic recrystallization (DRX) routes at 250, 300 and 350°C for achieving the highest volume fraction of fine grains at fracture

Route	Temperature, °C	Constant Strain Rate, s ⁻¹	V _f , ±5%	Average grain size, μm	Elongation-to-failure, ±5%
I	250	1 × 10 ⁻⁴	92	6.5	140
II	300	1 × 10 ⁻³	70	7.5	105
III	350	1 × 10 ⁻²	60	10.0	110

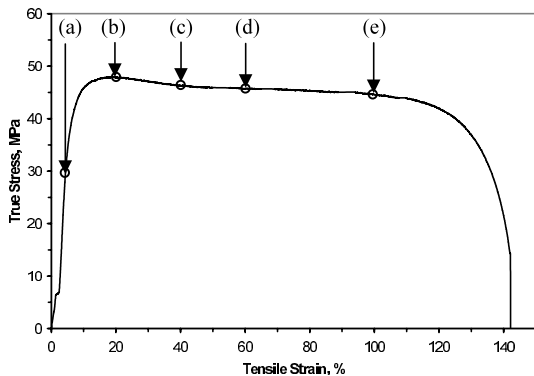


Fig. 3. True stress versus tensile strain curve showing steady state deformation under DRX conditions of 250 °C and $1 \times 10^{-4} \text{ s}^{-1}$. The microstructures and grain size distribution charts at points (a) to (e) are shown in Fig. 4.

than 400 °C and constant strain rate of $1 \times 10^{-4} \text{ s}^{-1}$ [9]. However, in this case, the formation of newly recrystallized fine grains during the initial stage of hot deformation has made steady state deformation possible even at 250 °C. The presence of a high percentage of fine grains has enabled grain boundary sliding (GBS) to act as the predominant deformation mechanism.

The above findings are similar to the deformation behavior of a rolled Mg–9Al–1Zn that also underwent DRX during the tensile test, as reported by Mohri et al. [6]. However, the rolled Mg–9Al–1Zn showed apparent strain softening until fracture and did not display any steady state deformation behavior whereas the rolled Mg–3Al–1Zn alloy exhibited apparent steady state deformation. This difference in deformation behavior could be due to the fact that Mg–9Al–1Zn contains an additional 6 wt.% of aluminium alloying elements when compared to Mg–3Al–1Zn. At this stage, the role of Al on the flow is thought to be associated to the formation of filaments among the equiaxial grains during GBS [10].

Fig. 4 depicts the evolution of recrystallized microstructures with the corresponding grain size distribution charts. At the beginning of the deformation process, i.e. $\epsilon = 5\%$, because of static grain growth during heating-up process, the as-received microstructure had transformed into a coarse-grained structure whose average size was $\approx 25 \mu\text{m}$ as shown in Fig. 4(a). The percentage of fine

grains was merely 18.6% while the remaining 81.4% was more than $10 \mu\text{m}$. The grain size distribution chart in Fig. 4(i) exhibits a highly scattered grain size distribution ranging from 2 to $85 \mu\text{m}$.

At $\epsilon = 20\%$, the coarser grain boundaries appeared serrated, as shown in Fig. 4(b) and a small amount of fine recrystallized grains started to nucleate along grain boundaries and at triple junctions. As a result, the percentage of fine grains increased to 31% and the average grain size reduced to $\approx 15.2 \mu\text{m}$. The corresponding distribution chart in Fig. 4(ii) shows that more grains accumulated within the $1 \sim 5 \mu\text{m}$ range. These were newly nucleated grains and therefore it is evident that dynamic recrystallization initiated right after the peak stress, as can be clearly identified as ‘Point (b)’ in Fig. 3. This observation is also consistent with the findings of other researchers [16,17] who investigated DRX of superplastic materials.

Fig. 4(c) depicts the microstructure at $\epsilon = 40\%$, where the amount of fine DRX grains had greatly increased to $\approx 68.9\%$. These grains were found encompassing the original coarser grain boundaries and the average grain size was $\approx 10 \mu\text{m}$. Apparently, as the strain increases, fine DRX grains proceeded to cover more of the original microstructure.

When $\epsilon = 60\%$, DRX grains basically covered the entire microstructure resulting in about 85% of fine grains. DRX grains with an average size of $6 \mu\text{m}$ were homogeneously distributed, as depicted in Fig. 4(d). The corresponding distribution chart in Fig. 4(iv) shows that out of the 85% of fine grains, the majority of them, i.e. 52% were tabulated within $1 \sim 5 \mu\text{m}$ range. At this strain level, coarser grains constituted only 15% of the microstructure. From these observations, it can be concluded that ‘complete’ recrystallization can be attained at $\epsilon = 60\%$. Also, it is interesting to note that from 60% strain and onwards, the change in terms of the percentage of fine grains attainable was minimal. The percentage of DRX grains was about $80 \pm 5\%$ and the average grain size was $7 \pm 1 \mu\text{m}$. The grain size distribution charts in Fig. 4(iv) and (v) also depict minimal change in terms of grain size distribution. Basically, after 60% strain, the microstructure has attained a steady state and hence does not display significant variation with strain. Grains that have coarsened due to dynamic growth are continuously replaced by new DRX grains, thus main-

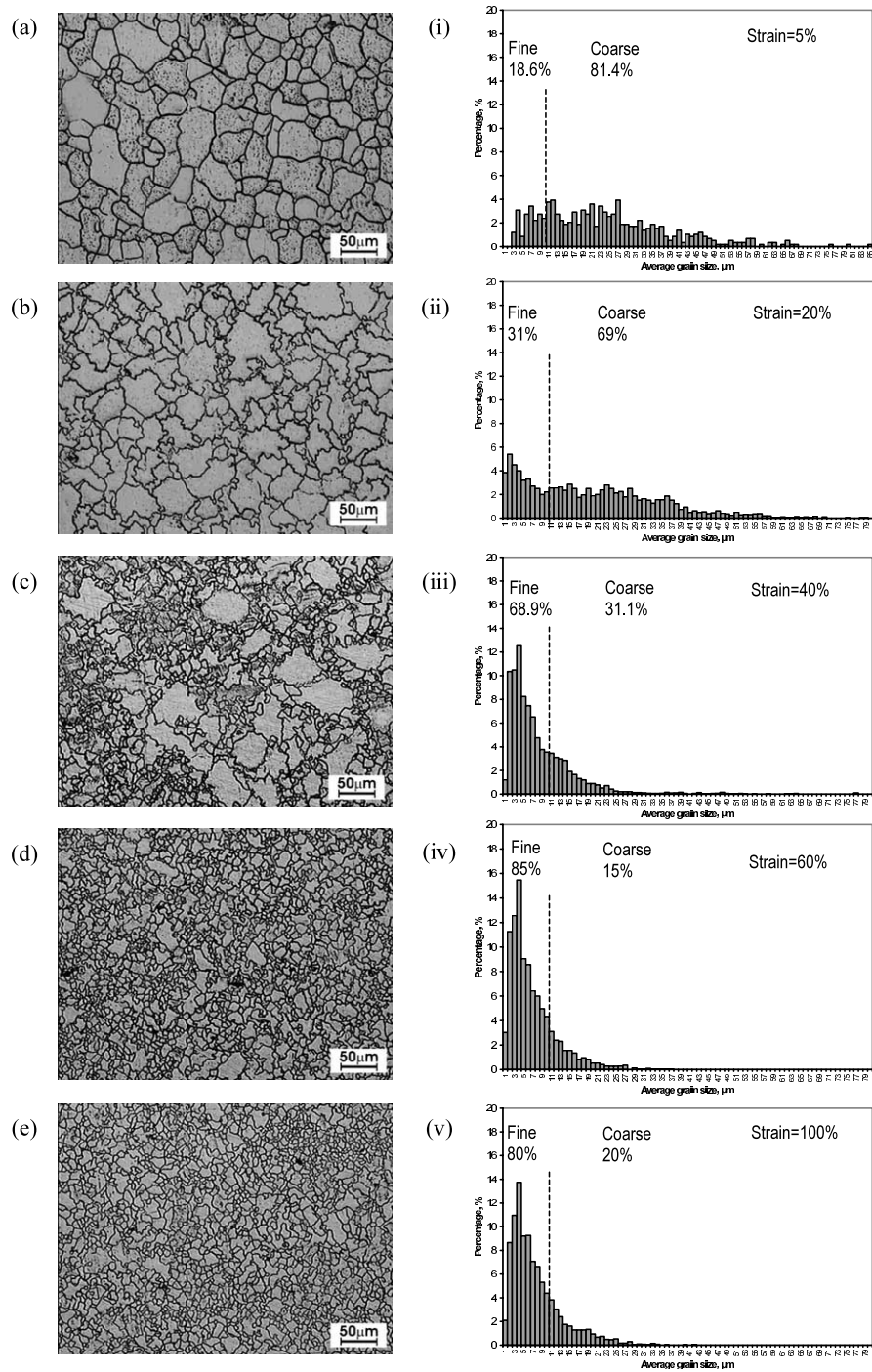


Fig. 4. Micrographs depicting typical microstructural evolution at: (a) 5%; (b) 20%; (c) 40%; (d) 60%; and (e) 100%, and their corresponding grain size distribution charts [(i) to (v)] for specimens tested at 250 °C and constant strain rate of $1 \times 10^{-4} \text{ s}^{-1}$. A minimum of 5000 individual grains was quantified to plot each distribution chart. Tensile axis was in the horizontal direction.

taining a high volume fraction of fine grains until fracture, as depicted in Fig. 5.

3.2. Dynamic recrystallization mechanisms

The internal grain structures as well as dislocation substructures of Mg–3Al–1Zn were examined under a TEM to investigate the DRX mechanisms. TEM

micrograph of a specimen strained to 40% under the optimum DRX condition is presented in Fig. 6. The serrated grain boundary and fine subgrains can be clearly recognized. Dislocation structures can also be identified near the subgrain boundaries and within the subgrains.

Well defined subgrains can be identified near the serrated grain boundary. In spite of that, the morphol-

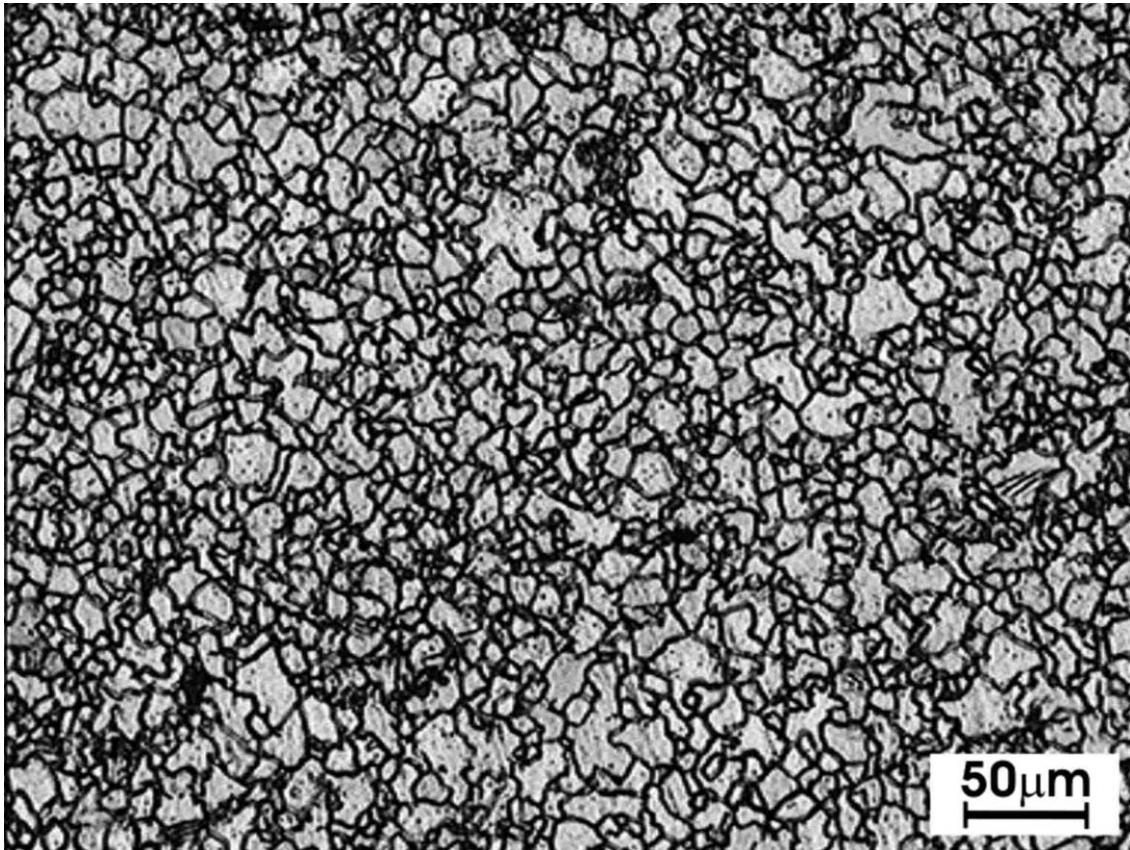


Fig. 5. Micrograph showing the high volume fraction of fine grains along the gauge of a specimen which fractured at 140%, under the test conditions of 250 °C and constant strain rate of $1 \times 10^{-4} \text{ s}^{-1}$. The tensile axis was in the horizontal direction.

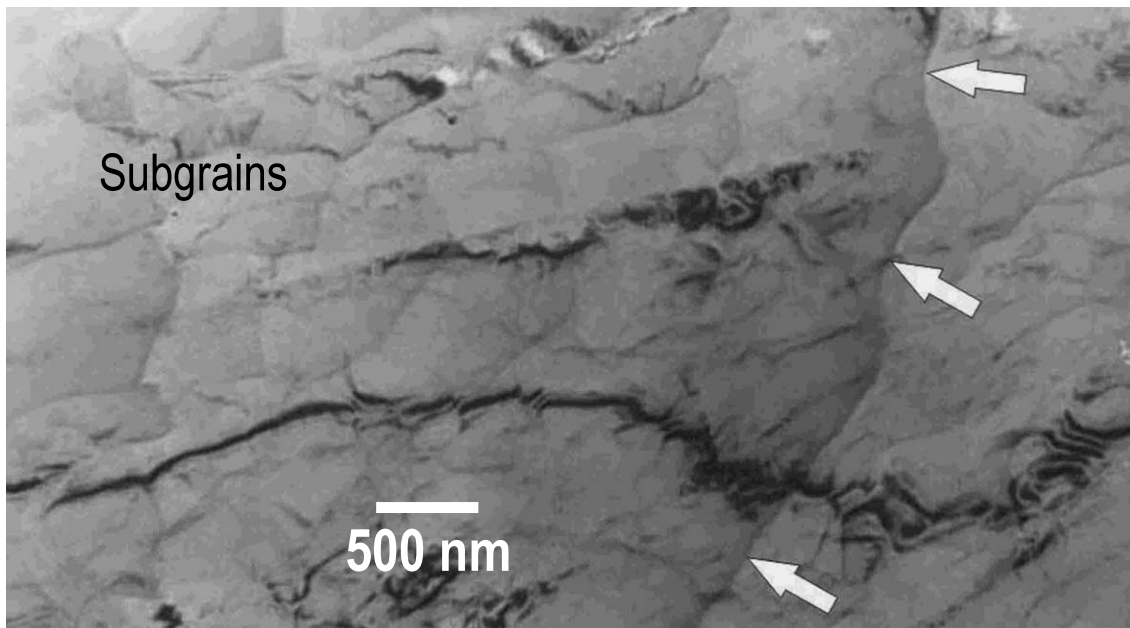


Fig. 6. TEM micrograph showing the subgrain structure and serrated grain boundary (indicated by the white arrows) in a specimen strained to 40% at 250 °C and constant strain rate of $1 \times 10^{-4} \text{ s}^{-1}$.

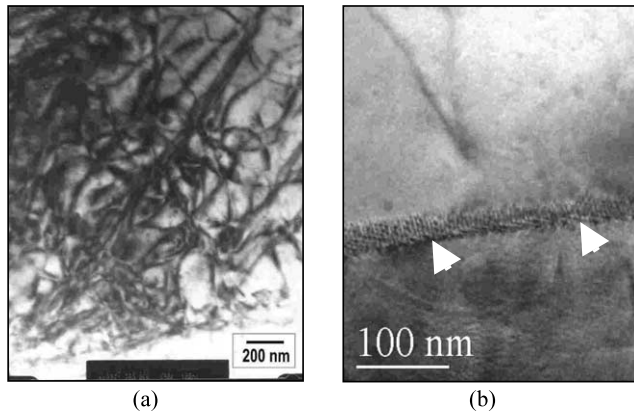


Fig. 7. (a) Fine dislocation cell structures within the grain interior. (b) Higher magnification micrograph depicting a dislocation array. The specimen was strained to 40% under test conditions of 250 °C and constant strain rate of $1 \times 10^{-4} \text{ s}^{-1}$.

ogy of the substructures becomes distinctly different far from the serrated boundary. The coarser grain interior consists of cells of tangled dislocation walls, as depicted in Fig. 7(a). These fine dislocation cell structure can convert to subgrain structure by a recovery process. From the above observations, it can be inferred that subgrains are first developed in the vicinity of the serrated grain boundaries and as deformation progresses, subgrain structure will form over the whole volume of the grain through the conversion of dislocation cell walls into subgrain boundaries.

An interesting feature seen at the early stage of DRX for rolled Mg–3Al–1Zn is the formation of serrated or corrugated grain boundaries especially among the coarser grains, as shown in Fig. 4(b) and Fig. 6. During the plastic deformation of a polycrystalline material, grain boundaries will act as obstacles to impede the motion of dislocations. The lattice dislocations which interact with the grain boundaries will produce new line defects which are called extrinsic grain boundary dislocations (EGBDs) [18]. Due to the presence of EGBDs within the grain boundaries, they contain higher energy and hence, always exist in a non-equilibrium state. Plastic deformation continuously introduces new dislocations into the grains, therefore increasing the EGBD density. However, since the deformation is carried out at elevated temperatures, dynamic recovery of grain structures also takes place simultaneously.

Sangl and Tangri [19] have previously explained the changes in the EGBD density by the two competing processes, that is the absorption of lattice dislocations and their annihilation with the grain boundary structure. Fig. 8 shows the absorption of dislocations by the subgrain boundaries. Serrated boundaries occur when the density of dislocations entering the grain boundaries exceeds their absorption capacity or when the process of lattice dislocation absorption requires an incubation time [20]. Under one of these circumstances, the

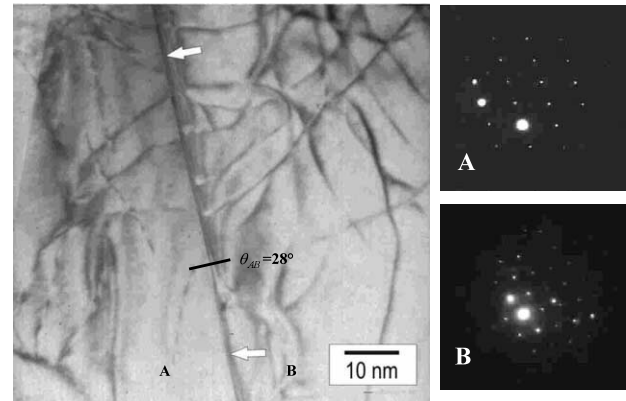


Fig. 8. TEM micrographs of two neighboring subgrains A and B taken from a DRX specimen strained to 60% at 250 °C and $1 \times 10^{-4} \text{ s}^{-1}$. The absorption of lattice dislocations into the subgrain boundaries can be clearly observed. Misorientation angle, θ_{AB} estimated from the diffraction patterns is also shown. The white arrows indicate the location of subgrain boundary.

excessive lattice dislocations will pile up and subsequently generate a local stress concentration on the grain boundary, hence resulting in the formation of serrated boundaries. To further reduce the stress concentration, the pile-up dislocations in the vicinity of the grain boundaries rearrange themselves to form groups of small-angle boundaries and dislocation cell structures (Fig. 7), which leads to the development of subgrains in the area adjacent to the serrated grain boundaries [21,22]. Sangl and Tangri [19] also proposed a model for the annihilation of EGBDs which suggests that the annihilation rate is dependent upon the grain boundary length. Owing to the fact that coarser grains possess larger grain boundary lengths, they will therefore have a greater tendency to develop serrated grain boundaries. These observations explain why the dynamically recrystallized grains in Fig. 4(b) and (c) initially developed along the coarser and serrated grain boundaries.

Dynamic recrystallization can be classified into either continuous or discontinuous recrystallization. In general, during continuous recrystallization, dislocations will remain in the recrystallized grains whereas discontinuous recrystallization removes dislocations through the sweeping action of high angle boundaries. Continuous recrystallization is also considered as a recovery dominated process where there will be progressive increase in boundary misorientation and conversion of low angle boundaries into high angle boundaries.

In the current work, dislocations can be observed in the recrystallized grain interior as well as along the grain boundaries. TEM studies showed that well defined subgrain boundaries were rarely observed in the recrystallized grains interior, inferring that subgrain boundary misorientation increased during high temperature deformation and low angle grain boundaries transformed into high angle boundaries. Evidence of this transforma-

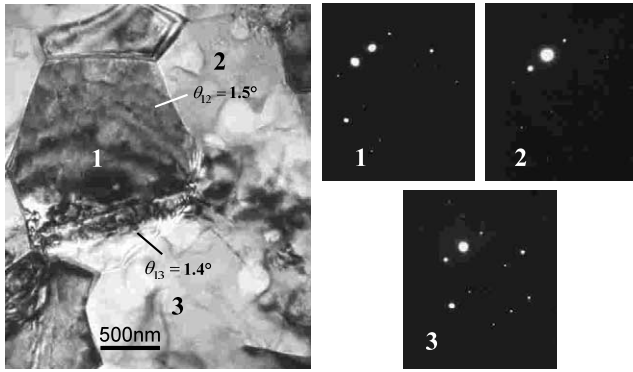


Fig. 9. TEM micrograph of an undeformed specimen and the corresponding diffraction patterns of the grains, denoted as 1 to 3. The misorientation angles between the neighboring grains are small, ranging from $1 \sim 2^\circ$.

tion can be found on the TEM micrographs shown in Fig. 8 and Fig. 9. Fig. 9 depicts the internal grain structure of an undeformed specimen (i.e. as-received alloy). Three neighboring grains were identified and designated as 1 to 3 and their corresponding diffraction patterns were obtained. These diffraction patterns were acquired using Selected Area Diffraction (SAD). The angle between the zone axes of two adjacent grains signifies the misorientation of the boundary. However, since this method does not take into account the lattice rotation around the zone axis, the calculated value will be less than the actual boundary misorientation. From their diffraction patterns, the misorientation angles θ_{12} and θ_{13} were estimated to range from $1 \sim 2^\circ$, implying that they possessed small misorientation angles and low angle boundaries. On the contrary, the two neighboring subgrains (Fig. 8) in a dynamically recrystallized and deformed specimen, designated as A and B, possessed a high misorientation angle θ_{AB} of approximately 28° , as determined from the diffraction patterns. By comparing these two TEM micrographs, we can conclude that the large increase in grain misorientation observed was attributed to dynamic continuous recrystallization (DCRX).

It is important to note that the TEM micrographs do not reveal any signs of precipitates/particles within the internal microstructures or on the grain boundaries. The absence of precipitates is due to the fact that $\text{Mg}_{17}\text{Al}_{12}$ will only form when the Al to Zn ratio is greater than 3:1 [23]. Thus, there are no precipitates pinning the subgrain boundaries or the dislocation substructures. Previous studies [24–27] in dynamic recrystallization of aluminium alloys emphasized the importance of stable particles such as Al_3Zr and Al_3Sc in stabilizing the subgrain structures during continuous recrystallization. Also, it has been reported [28] that DRX does not readily take place in aluminium alloys due to the high stacking fault energy, inferring that the grain boundaries need to be stabilized by fine and stable particles.

Nevertheless, this was not the case for the rolled Mg–3Al–1Zn alloy since dynamic continuous recrystallization has occurred without the need for precipitates to stabilize the subgrains.

According to Ion and his coworkers [29], dynamic recrystallization of Mg–0.8wt.%Al alloy during hot deformation can be attributed to the constraint imposed by the lack of easily activated slip systems. This is plausible since HCP crystal structure in magnesium alloys generally has very limited number of slip systems. Even though the pyramidal and prismatic slip systems [23] become operative at high temperatures, the number of active slip systems is still relatively limited in contrast to aluminium alloys which possess face-centered cubic (FCC) crystal structure. The second reason is because unlike aluminium, magnesium has low stacking fault energy, which is in the range of 60 to 78 mJ/m^2 for pure magnesium [30]. Another possible reason can be ascribed to the high grain boundary diffusion rate of magnesium when compared to aluminium [31]. Therefore, as has been depicted in figure, the pile-up dislocations at subgrain boundaries can be absorbed by these boundaries hence resulting in an accelerated recrystallization process. These three reasons explain why the absence of precipitates does not hinder dynamic continuous recrystallization from taking place in the rolled Mg–3Al–1Zn alloy.

4. Conclusions

Grain refinement of a rolled Mg–3Al–1Zn alloy sheet can be attained via dynamic recrystallization (DRX). The optimum DRX condition was found to be at 250 °C and constant strain rate of $1 \times 10^{-4} \text{ s}^{-1}$.

At optimum DRX conditions, 85% of homogeneous and equiaxial grains with an average grain size of 6 μm is obtained. These fine grains with high angle boundaries are capable of grain boundary sliding during superplastic deformation.

TEM examinations confirmed that the DRX phenomenon is attributed to dynamic continuous recrystallization where there is progressive increase in grain boundary misorientation and conversion of low angle boundaries into high angle boundaries.

During DRX, subgrains are first developed in the vicinity of the serrated grain boundaries and as deformation progresses, subgrain structure will form over the whole volume of the grain through the conversion of dislocation cell walls into subgrain boundaries.

The presence of precipitates is not required for dynamic recrystallization in Mg–3Al–1Zn alloy sheet. This can be ascribed to the constraint imposed by the lack of easily activated slip systems in hexagonal close-packed crystal structure, the low stacking fault energy

and also the high grain boundary diffusion rate of magnesium.

References

- [1] R.S. Busk, *Magnesium Products Design*, Marcel Dekker, Inc, NY, USA, 1987, pp. 12–37.
- [2] J.C. Tan and M.J. Tan, 'Superplastic Magnesium Alloy for Sporting and Leisure Equipments', *Proceedings of Symposium on Materials and Science in Sports*, F.H. (Sam) Froes and S.J. Haake, eds., TMS, Coronado, California, 22–25 April 2001, pp. 95–104.
- [3] B.M. Closset, J.F. Pery, S.A. Timminco, C. Bonjour, P.A. Moos, V. Ecole, in: B.L. Mordike, K.U. Kainer (Eds.), *Magnesium Alloys and their Applications*, Werkstoff-Informationsgesellschaft, Frankfurt, 1998, pp. 195–200.
- [4] H. Takuda, T. Yoshii, N. Hatta, *J. Mater. Process. Technol.* 89–90 (1999) 135.
- [5] H. Takuda, S. Kikuchi, N. Hatta, *J. Mater. Sci.* 27 (1992) 937.
- [6] T. Mohri, M. Mabuchi, N. Nakamura, T. Asahina, H. Iwasaki, T. Aizawa, K. Higashi, *Mat. Sci. Eng. A290* (2000) 139.
- [7] T. Takasugi, Y. Watanabe, H. Inoue, *Scripta Mater.* 43 (2000) 485.
- [8] I.I. Novikov, V.K. Portnoy, A.O. Titov, D.Yu. Belov, *Scripta Mater.* 42 (2000) 899.
- [9] J.C. Tan and M.J. Tan, Superplastic deformation behavior in Mg–3Al–1Zn alloy sheet, submitted to *Mater. Sci. Eng. A* (2001).
- [10] J.C. Tan and M.J. Tan, Superplasticity and grain boundary sliding characteristics in two stage deformation of Mg–3Al–1Zn alloy sheet, *Mater. Sci. Eng. A* (in press).
- [11] *Annual Book of ASTM Standards*, Section 3: 03.01, E112-96, p. 229, American Society of Testing and Materials, Philadelphia, PA (1998).
- [12] T.G. Nieh, J. Wadsworth, O.D. Sherby, *Superplasticity in Metals and Ceramics*, Cambridge University Press, 1996, p. 22.
- [13] T.G. Langdon, *Metall. Trans.* 13A (1982) 689.
- [14] A.K. Ghosh, C.H. Hamilton, *Metall. Trans.* 10A (1979) 699.
- [15] C.H. Caceres, D.S. Wilkinson, *Acta Metall.* 32 (1984) 415.
- [16] K.Y. Kim, S. Hanada, T. Takasugi, *Scripta Mater.* 37 (1997) 1053.
- [17] K.Y. Kim, S. Hanada, T. Takasugi, *Acta Mater.* 46 (1998) 3593.
- [18] R.W. Balluffi, Y. Komen, T. Schober, *Surf. Sci.* 31 (1972) 69.
- [19] S. Sangl, K. Tangri, *Metal. Trans.* A20 (1989) 479.
- [20] R.Z. Valiev, O.A. Kaibyshev, Sh.Kh. Khannanov, *Phys. Status Solidi A52* (1979) 447.
- [21] J.L. Lytton, C.R. Barret, O.D. Sherby, *Trans. AIME* 233 (1965) 1399.
- [22] S. Hashimoto, B. Baudelet, *Scr. Metall.* 23 (1989) 1855.
- [23] M.A. Michael, H. Baker (Eds.), *ASM Specialty Handbook: Magnesium and Magnesium Alloys*, ASM International, 1999.
- [24] T.G. Nieh, L.M. Hsiung, J. Wadsworth, R. Kaibyshev, *Acta Mater.* 46 (1998) 2789.
- [25] T.R. McNelly, E.W. Lee, M.E. Mills, *Metall. Trans.* 17A (1986) 1035.
- [26] N. Furushiro, S. Hori and Y. Mikaye, *Proc. International Conference on Superplasticity in Advanced Materials*, In: S. Hori, M. Tokizawa and N. Furushiro (Eds.), *The Japan Soc. Res. in Superplasticity*, Tokyo (1991) pp. 557.
- [27] H.J. McQueen, E. Evangelista, J. Bowles, G. Crawford, *Met. Sci.* 18 (1984) 395.
- [28] C.M. Sellers, *Philos. Trans. R. Soc.* A288 (1978) 147.
- [29] S.E. Ion, F.J. Humphreys, S.H. White, *Acta Mater.* 30 (1982) 1909.
- [30] D.H. Sastry, Y.V.R.K. Prasad, K.I. Vasu, *Scr. Met.* 3 (1969) 927.
- [31] M. Mabuchi, K. Higashi, *Acta Mater.* 44 (1996) 4611.